The function of the alula on engineered wings: a detailed experimental investigation of a bioinspired leading-edge device

Bioinspiration & Biomimetics

PAPER

The function of the alula on engineered wings: a detailed experimental investigation of a bioinspired leading-edge device

RECEIVED
25 February 2019

REVISED
20 June 2019

ACCEPTED FOR PUBLICATION
25 July 2019

PUBLISHED
29 August 2019

Mihary R Ito, Chengfang Duan and Aimy A Wissa[1]

Department of Mechanical Science and Engineering, University of Illinois at Urbana-Champaign, 105 S. Mathews Ave., Urbana, IL 61801, United States of America

[1] Author to whom correspondence should be addressed.

E-mail: awissa@illinois.edu

Keywords: leading-edge device, alula, stall-mitigation, lift improvement, low Reynolds number flight

Abstract

Birds fly in dynamic flight conditions while maintaining aerodynamic efficiency. This agility is in part due to specialized feather systems that function as flow control devices during adverse conditions such as high-angle of attack maneuvers. In this paper, we present an engineered three-dimensional leading-edge device inspired by one of these specialized groups of feathers known as the alula. Wind tunnel results show that, similar to the biological alula, the leading-edge alula-inspired device (LEAD) increases the wing's ability to maintain higher pressure gradients by modifying the near-wall flow. It also generates tip vortices that modify the turbulence on the upper-surface of the wing, delaying flow separation. The effect of the LEAD location and morphology on lift production and wake velocity profile are investigated using force and hot-wire anemometer measurements, respectively. Results show lift improvements up to 32% and 37% under post and deep stall conditions, respectively. Despite the observed drag penalties of up to 39%, the aerodynamic efficiency, defined as the lift-to-drag ratio, is maintained and sometimes improved with the addition of the LEAD to a wing. This is to be expected as the LEAD is a post-stall device, suitable for high angles of attack maneuvers, where maintaining lift production is more critical than drag reduction. The LEAD also accelerates the flow over the wing and reduces the wake velocity deficit, indicating attenuated flow separation. This work presents a detailed experimental investigation of an engineered three dimensional leading-edge device that combines the functionality of traditional two dimensional slats and vortex generators. Such a device can be used to not only extend the flight envelope of unmanned aerial vehicles (UAVs), but to also study the role and function of the biological alula.

Nomenclature

α	Wing angle of attack (AoA)
α_{STALL}	Wing stall AoA
β	LEAD AoA relative to wing chord line
γ	LEAD tip deflection angle
b	Wing span
b_A	LEAD span
c	Wing chord
c_A	LEAD chord
C_D	Finite wing (3D) drag coefficient
C_{D0}	Finite baseline wing (3D) drag coefficient
ΔC_D	The difference in C_D between the baseline wing and the wing-LEAD assembly
C_l	Airfoil (2D) lift coefficient
C_L	Finite wing (3D) lift coefficient
C_{L0}	Finite baseline wing (3D) lift coefficient
ΔC_L	The difference in C_L between the baseline wing and the wing-LEAD assembly
Re	Reynolds number
s	Wing semi-span
U	Averaged velocity in the streamwise direction
U_∞	Freestream velocity
x/c	Airfoil chord location, normalized by the wing chord
y/s	Hot-wire probe spanwise location, normalized by the wing semi-span
y_A/s	LEAD root to wing root distance (%)
z/c	How wire probe vertical location, normalized by the wing chord

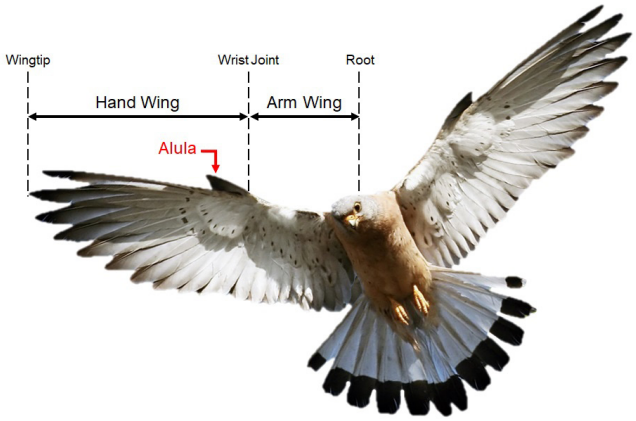

Figure 1. A bird during an approach maneuver with the alula on each side of the wing deployed (Photo by Satya Tiwari/Pixabay). The root of the alula is located at the wrist joint, which is the intersection between the hand wing and the arm wing. The rest of the alula extends outboard of the wrist.

1. Introduction

Unmanned aerial vehicles (UAVs) have proliferated in the civilian sector over recent years. Applications include aerial imaging, search and rescue, work-site inspection, cargo delivery, and more. Such applications are mission-driven and require maneuverable UAVs that can fly in confined spaces and near humans. Therefore, mission adaptability, defined as the ability to safely and successfully complete multiple tasks using the same vehicle, is an important design factor. However, mission adaptability is limited for vehicles classified by scale as mini-UAVs [1]. These vehicles are close in size to birds, allowing them to be launched by hand, and they fly at low altitudes and low speeds [2]. Due to these factors, these vehicles operate at low Reynolds numbers. Under these flight conditions, the lift generated by a wing is greatly reduced, and the aerodynamic efficiency is diminished (i.e. for a given amount of lift, more drag is generated). According to aerodynamic principles, a wing produces more lift when its angle of attack (AoA or α) is increased. However, this angle can only be increased to the stall AoA, α_{STALL}, beyond which lift generation is limited by flow separation [3, 4]. Stall is especially a concern during high angle of attack (AoA) maneuvers, such as short distance take-off and landing, hovering, and perching. The ability of mini-UAVs to complete these maneuvers without the loss of the ability to produce lift crucial for mission adaptability. Therefore, alternative methods to generate high lift at low Reynolds numbers and at high AoAs are necessary to achieve this goal.

In nature, mission adaptability is apparent in avian flight as birds engage in complex maneuvers using the same flight apparatus. Both bird and mini-UAVs operate under low Reynolds number conditions [5]. Yet, the flight envelope of birds exceeds that of UAVs [2]. Birds achieve mission-adaptability by morphing their wings and feathers during flight maneuvers [6]. For instance, bird wings are equipped with a set of small feathers near the leading-edge, known as the alula. When deployed, the alula enables the wing to sustain the lift necessary to fly at low speeds and high AoAs [3, 7, 8].

This paper presents a detailed investigation of the function of a leading-edge alula-inspired device (LEAD) on lift-enhancement and stall-mitigation in finite wings with low to moderate aspect ratios operating at low Reynolds numbers. More specifically, we will answer the following questions:

- What is the effect of the LEAD on lift and drag production as well as on the wake profile of a three-dimensional wing section?
- What is the sensitivity of the LEAD performance to its deployment parameters?
- Are there apparent interactions between the LEAD and the base wing tip vortices?

2. Background

2.1. Bird wing and alula morphology

Equipped with strong skeletal components, light muscles, and flexible feathers, wings are the most important components of a bird's flight apparatus. In general, a bird wing can be divided into two distinct parts: the arm wing and the hand wing. The arm wing consists of bones, making its airfoils thick and suitable for low-speed flight. The hand wing is mainly comprised of feathers, making it thin and prone to stall at low speeds [9]. A detailed description of the morphology of the arm and hand wings is presented by Videler in [10]. The two parts of the wing intersect at the wrist joint, as shown in figure 1. The alular digit, or the thumb, is situated at this intersection and near the wing leading-edge. The digit is covered with a set of 2 to 6 feathers to form the alula structure, also known as bastard wing. The joint at the alula root allows deflections both away from the wing leading-edge (forward) and away from the wing upper surface (upward) [10]. In cruising conditions, the alula

Table 1. Morphology database of bird species with type D (high-lift) wings and respective alulae. Adapted from Alvarez *et al* [13].

Bird species	Alula length L_a (m)	Wing aspect ratio AR	Alula root to wing root distance $1 - L_c/L_w$	Alula length to bird span ratio $2L_a/L_b$
Bubulcus ibis	0.07	7.239	0.390	0.169
Ciconia ciconia	0.14	8.402	0.411	0.146
Milvus migrans	0.11	7.465	0.323	0.158
Gyps fulvus	0.16	6.345	0.352	0.144
Hieraaetus pennatus	0.11	7.327	0.327	0.182
Falco naumanni	0.05	8.03	0.300	0.152
Tyto alba	0.07	7.689	0.341	0.156
Otus scops	0.04	5.886	0.391	0.194
Athene noctua	0.04	5.784	0.304	0.188
Strix aluco	0.07	6.198	0.366	0.175
Average	0.09	7.004	0.351	0.166

remains stowed along the wing upper surface and leading-edge. During maneuvers such as take-off, landing, and perching, the alula has been observed to deploy [10].

Based on morphology, function, and flight performance, Saville *et al* classified bird wings into four types (A, B, C, and D) as detailed in [11]. Among the four types, the alula is commonly found in type A (elliptical) and type D (high-lift) wings. Both types have low to moderate aspect ratios, are adapted to frequent take-offs and landings, and for efficient flight at low to moderate speeds. Type D wings are best-suited for birds of prey, which frequently dive, perch, and carry payload. Airfoils found in this wing type are noticeably cambered to produce high lift [12].

Alvarez *et al* [13] investigated the characteristics of alulae on various bird species equipped with the four types of wings and compiled them in a detailed database. The findings of this study confirmed that birds equipped with type D wings have the most pronounced alulae. Table 1 shows a summary of dimensions of type D wings and alulae for the species evaluated. The length, or span, of the alula for high lift wings ranges from 14.4% to 19.4% of the full wing span. The alula root is located between 28.6% and 41.4% semi-span away from the wing root.

Wing planforms similar to type D wings are desirable for mini-UAV design due to their maneuverability and high payload capacity. Since birds equipped with Type D wings depend on their pronounced alulae to achieve complex maneuvers, it is worth investigating an alula-inspired device to improve mission adaptability in mini-UAVs.

2.2. The alula and other engineered leading-edge devices

A number of experimental studies have been conducted by biologists on the wings of live or dead birds to understand the function of the alula in avian flight [7–9, 14]. Austin *et al* observed in a wind tunnel test that the alula does not deflect at low AoAs, but it lifts away from the wing upper surface near stall conditions [9]. Lee *et al* also conducted various experiments on live and dead birds and concluded that once the alula deploys, birds are able to complete more complex maneuvers and produce more lift during a given flight task. This study also showed a drag penalty due to the deployment of the alula [7]. Results from a different study show that a deployed alula causes the wing boundary layer to remain attached to the wing upper surface at high AoAs, thus maintaining lift production over extended flight conditions [8]. When investigating the effect of the alula on the flow field, Lee *et al*. also showed that a streamwise vortex is shed by the tip of the alula on the upper surface of the wing [7]. Additionally, the flow behind a wing with a deployed alula is faster compared to a wing without an alula [9].

On full-scale aircrafts, high-lift devices are components added to the wings to augment lift generation capacity. These devices are most frequently used when an aircraft is flying slower than cruising conditions such as during take-off and landing [15]. High-lift devices either modify the chord and camber of the lifting surface or the boundary layer surrounding it [16]. Devices that currently modify the wing's chord and camber to delay stall include trailing edge (TE) flaps [17]. Devices that modify the flow surrounding the wing include vortex generators, which create vortices that energize the boundary layer over the upper surface [18]. Aircraft wings are also sometimes equipped with leading-edge (LE) slats, which modify the adverse pressure gradient on the wing's airfoil such that they are less prone to stall. Slats and vortex generators are well-suited for full-scale aircraft that operate at high Reynolds number (10^6 or higher). They are large, heavy, and are usually actuated by complex mechanisms. To date, further investigation is necessary to design adequate high lift devices for small-scale UAVs operating at low Reynolds numbers (around 10^5).

An engineered alula (LEAD) was first implemented as a lift enhancement and stall mitigation device on a 2D wing by the authors in [19, 20]. These experimental studies have shown that a 2D wing equipped with the LEAD produces more lift and reduces the velocity deficit in its wake at high AoAs. Particle image velocimetry (PIV) results (figure 2) have shown faster flow in the

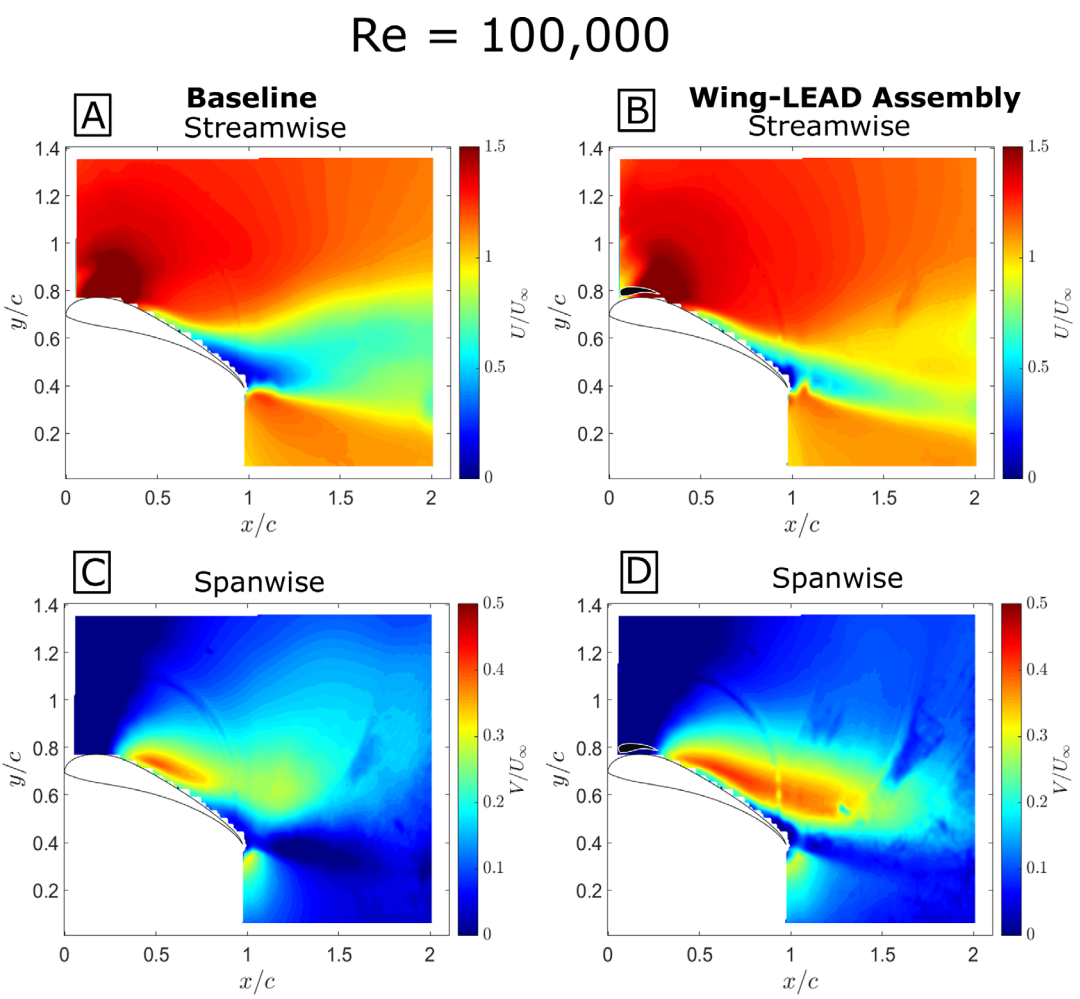

Figure 2. The effects of a LEAD wing on the velocity distribution around a 2D wing. A-B: in the streamwise direction, the addition of the LEAD reduces separation and the momentum deficit in the wake. (C) and (D): in the spanwise direction, the LEAD generates flow of a higher velocity indicating the presence of a vortex [21].

wake both in the streamwise and spanwise directions. Faster streamwise flow closer to the airfoil surface indicates separation alleviation, whereas faster spanwise flow indicates the presence of a tip vortex generated by the LEAD [21]. Since the alula is typically found on birds with low and moderate aspect-ratios, a 2D experiment gives an insightful but incomplete picture of the effects of the LEAD on a lifting surface. Thus, the LEAD was implemented on a 3D wing for the first time by the authors in [22]. This study experimentally evaluated the effect of the LEAD spanwise location on lift production. On the numerical side, Sanders *et al.* studied the effects of an alula-inspired device on a 3D wing. The CFD results attributes the increase in lift to a change in the local pressure distribution around the wing and the alula. A local minimum pressure, indicating accelerated flow, is generated on the upper surface by the alula. The spanwise pressure gradient on the upper surface of the wing is also reduced, indicating high speed flow in the spanwise direction. The simulation results also show the presence of an alula tip vortex at high AoAs [23].

While engineered alula devices have been evaluated experimentally on 2D wings, and numerically studied on 3D wings, the effects of the morphology of the device on 3D wing aerodynamics have not been investigated. This paper presents a detailed experimental study of the effect of the LEAD deployment parameters on lift, drag, and aerodynamic efficiency, as well as a quantitative survey of the flow in the wake of a 3D wing.

3. Experimental methods

3.1. Experimental setup

The geometric parameters of the baseline wing and the LEAD were based on the morphology seen in birds with type D wings (table 1). The semi-span (distance from wing root to tip, $s = b/2$) and the chord (c) of the base wing were selected to be 220 mm and 80 mm, respectively. Therefore, the base wing aspect ratio (AR) was set to 5.5, which is considered moderate. The selected wing profile was the S1223, a cambered high-lift airfoil similar to typical type D wing profiles [12, 24].

The LEAD covered 15% of the wing span (30% of the semi-span), with a mean chord (c_A) of 18.7 mm and a span (b_A) of 67.5 mm. A model of the rectangular

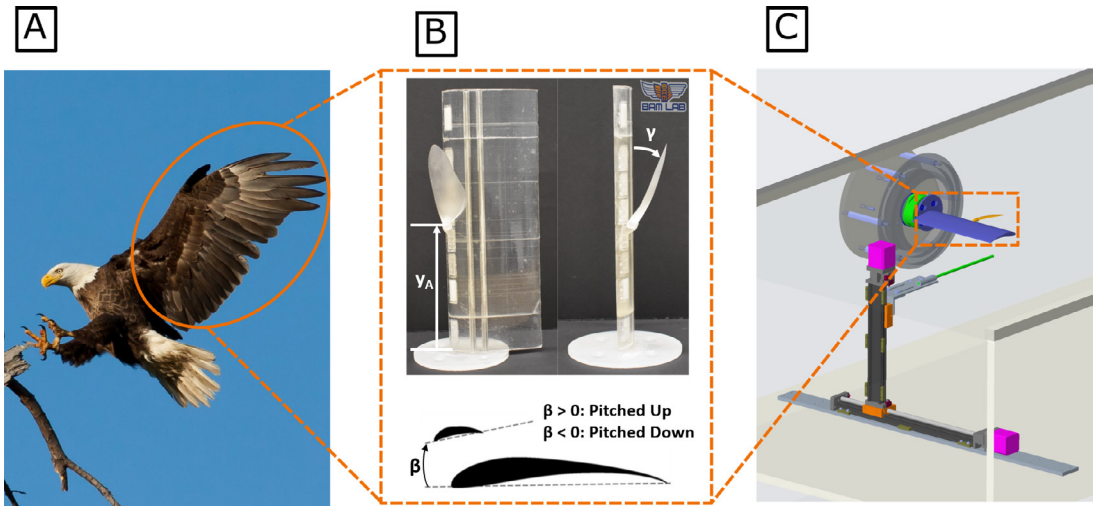

Figure 3. The bioinspired approach used to design the leading-edge alula-inspired device (LEAD). (A) A bald eagle with alula feathers deployed during a perching maneuver (Photo by skeeze/Pixabay). (B) The constructed wing-LEAD assembly. The dimensions and characteristics of the wing and LEAD test specimens are inspired by the morphology of high-lift wings. (C) The wind tunnel test section showing the experimental setup. The experiments conducted include integrated lift force measurements and wake boundary layer sampling.

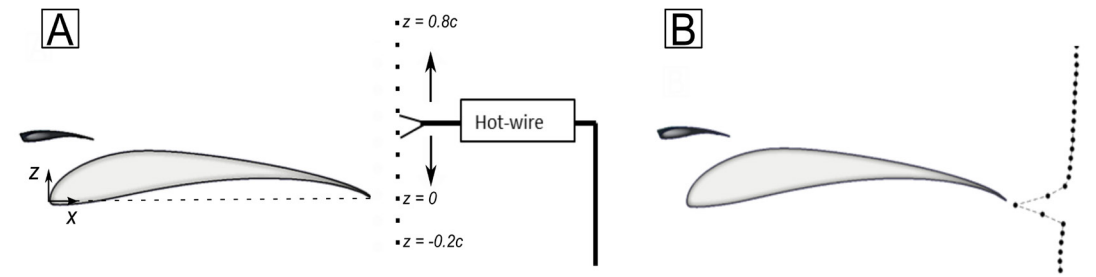

Figure 4. Experimental setup and configuration for hot-wire anemometer measurements. (A) The hot-wire probe was placed at $x/c = 1.125$ behind the trailing edge of the base wing and moved in the z direction from $z/c = -0.2$ to $z/c = 0.8$ to sample the boundary layer. (B) Example of velocity deficit profile expected from hot-wire measurements.

wing equipped with the LEAD is shown in figure 3(B). The LEAD profile was the NACA22, an airfoil commonly used in leading-edge devices. The LEAD has an elliptical chord distribution along the span and exhibits soft stall behavior in order to expand the operating envelope of the device to high wing AoAs.

A series of wind tunnel experiments were performed to characterize the aerodynamic effects of the LEAD on the wing at high AoAs. Measurements were taken for two configurations: a baseline wing (without a LEAD) and a wing equipped with a LEAD (wing-LEAD assembly). Experiments were conducted in a closed section, open-loop, constant pressure wind tunnel at the University of Illinois Urbana-Champaign as described in [22]. The test section of the wind tunnel closest to the inlet was chosen due to turbulence levels as low as 0.1%. The wind tunnel velocity was measured with a pitot-static tube placed 5 chord lengths ahead of the test wing. The pitot-static tube was aligned within $\pm 5^\circ$ along the freestream direction to ensure an uncertainty lower than 1%.

The tests consisted of force measurements to investigate the lift and drag generated by each configuration as well as hot-wire anemometer measurements to characterize the flow in the wake of the system. The aerodynamic forces generated by the wing-LEAD assembly were measured using an ATI Gamma 6-axis force/torque transducer at a sampling rate of 10 kHz for 3 s. This sensor has a high signal-to-noise ratio, a sensitivity of 1/160 N, and saturation levels of 35 N per force channel. The largest source of uncertainty in this experiment comes from the force transducer. The calibration for this instrument was supplied by the manufacturer at 1% of the full measurement scale for each force axis.

The wake boundary layer of the wing was sampled using a hot-wire probe placed at $x/c = 1.125$ downstream of the trailing edge as shown in figure 4. Six locations across the wingspan, as shown in figure 5, were chosen for wake survey. At each location, the probe was moved in the z direction from $z/c = -0.2$ (below the TE) to $z/c = 0.6$ (above the TE) in increments of 5 mm. The probe is made from a 5.0 μm tungsten wire, and connected to a DANTEC Dynamic data-collection system. Hot wire anemometer data was taken at 10 kHz for 5 s. The hot-wire probe was moved

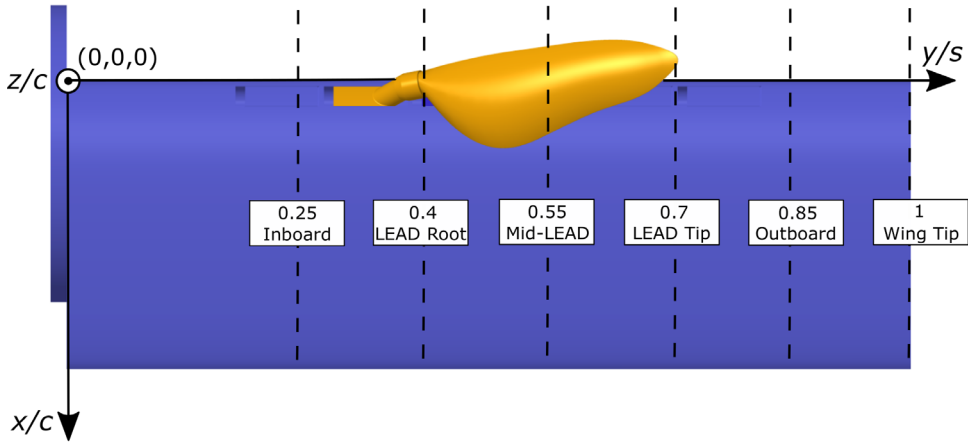

Figure 5. Hot-wire measurements were taken at the locations indicated on the wing. In the case shown, the LEAD root is located 40% semi-span away from the wing root.

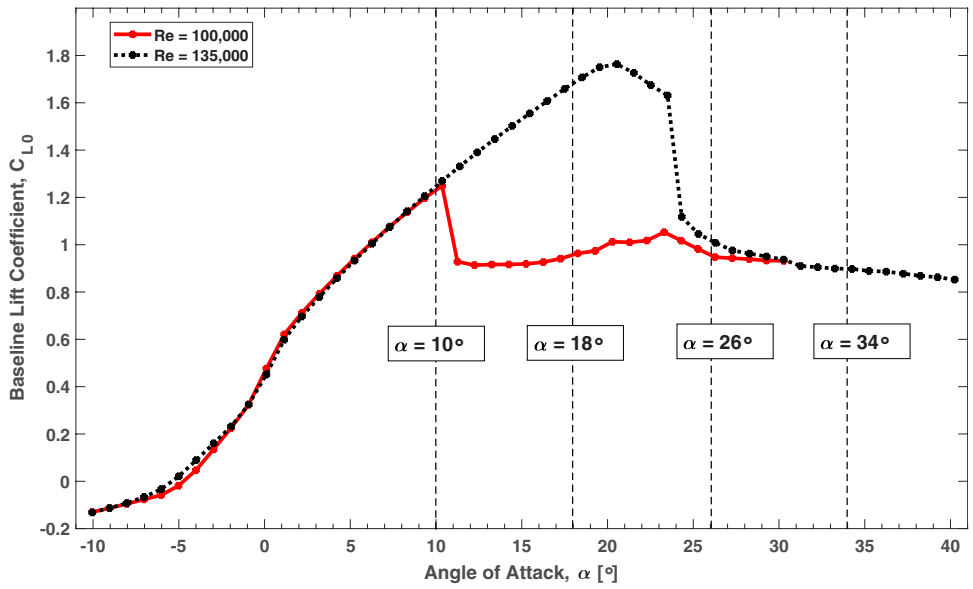

Figure 6. Experimental results showing the lift coefficient generated by the 3D rectangular wing at Re = 100 000 and Re = 135 000. The wing-LEAD assembly was tested at each AoA α marked.

upward and spanwise at fixed intervals using a traversing system to ensure repeatability.

3.2. Experimental matrix

The wind tunnel speed was varied to produce Reynolds number values of 100 000 and 135 000. In the baseline configuration, the wing AoA, α, was varied in increments of 1° from −10° to 30° for Re = 100 000 and from −10° to 40° for Re = 135 000. Based on the trends observed in the C_L versus α curves of the baseline wing, shown in figure 6, the AoAs evaluated during the wing-LEAD assembly runs were classified into three stall conditions as indicated in table 2.

For each Reynolds number and stall condition, the following LEAD deployment parameters were evaluated:

- y_A/s: Spanwise location of the LEAD root with respect to the wing root.
- γ: Deflection angle of the LEAD tip with respect to the wing upper surface.
- β: AoA of the LEAD relative to the main wing's chord.

These deployment parameters are illustrated in figure 3(B), and the values tested are shown in table 2. The configurations that resulted in the greatest improvements in lift (underlined in table 2) were evaluated using a wake surveying method using a hot-wire probe.

4. Results and discussion

4.1. Overall lift main effects

The percent difference between the lift coefficient generated by the wing-LEAD assembly and the baseline is plotted against the wing AoA in figure 7. This figure contains main effects plots (%C_L versus α, where

Table 2. Experiment matrix: lift and drag measurements were taken for all configurations. The configurations evaluated using hot-wire anemometry are underlined.

		Re = 100 000	Re = 135 000
Pre-Stall	α	10°	10°, 18°
	y_A/s	30%, 40%, 50%, 60%, 70%	30%, 40%, 50%, 60%, 70%
	β	−18°, −13°, −10°, −5°, 0°, 5°	−18°, −13°, −10°, −5°, 0°, 5°
	γ	4°, 13°, 22°	4°, 13°, 22°
Post-stall	α	**18°**	**26°**
	y_A/s	30%, **40%**, 50%, 60%, 70%	30%, 40%, **50%**, 60%, 70%
	β	−18°, −13°, −10°, **−5°**, 0°, 5°	−18°, **−13°**, −10°, −5°, 0°, 5°
	γ	4°, 13°, **22°**	4°, 13°, **22°**
Deep stall	α	**26°**	**34°**
	y_A/s	30%, 40%, 50%, **60%**, 70%	30%, 40%, **50%**, 60%, 70%
	β	−18°, −13°, −10°, **−5°**, 0°, 5°	−26°, −21°, −18°, **−13°**, −10°, −5°
	γ	4°, 13°, **22°**	4°, 13°, **22°**

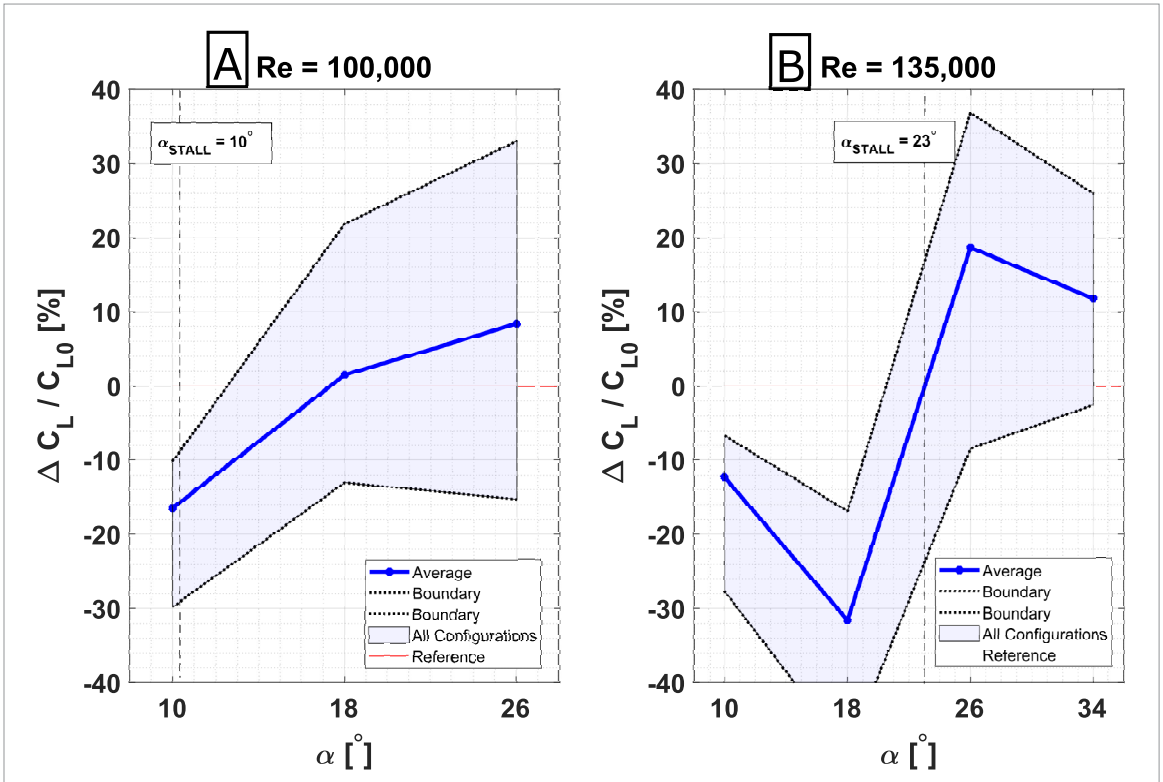

Figure 7. Main effects of wing AoA, α, on the percent difference between the lift generated by the wing equipped with the LEAD and the baseline wing. All configurations tested are contained in the shaded region. The effects of the following geometric parameters are also averaged: β, γ and LEAD root location. The LEAD decreases lift under pre-stall conditions and increases lift under post-stall and deep stall conditions.

$\%C_L = \Delta C_L/C_{L0}$); therefore, the contribution of only one parameter (α) is presented while the contribution of all other geometric parameters (β, γ, and y_A/s) is averaged. Additionally, the $\%C_L$ differences produced by all configurations tested are enclosed in the shaded region. To compute the lift coefficient C_L produced by the wing-LEAD assembly, the wetted area of both the wing and the LEAD were considered. Overall, the results show that the LEAD reduces lift under pre-stall conditions for the majority of the configurations ($\alpha < 18°$). At pre-stall, the flow is mostly attached and a favorable pressure gradient is present near the leading-edge. Therefore, adding the LEAD disturbs the pressure suction peak and reduces the overall lift produced by the wing. Once the AoA is increased into the post-stall region, the wing-LEAD assembly generates on average 1.5% more lift than the baseline at Re = 100 000 (Post-stall $\alpha = 18°$) and 12.9% at Re = 135 000 (Post-stall $\alpha = 26°$). Additionally, the majority of the configurations represented in the shaded region generated a positive percent difference. Greater improvements are obtained under deep stall conditions. On average, the LEAD enhances the lift coefficient by 8.4% at Re = 100 000 (Deep stall $\alpha = 26°$) and 11.8% at Re = 135 000 (Deep stall $\alpha = 34°$). Based on geometry and characteristics of

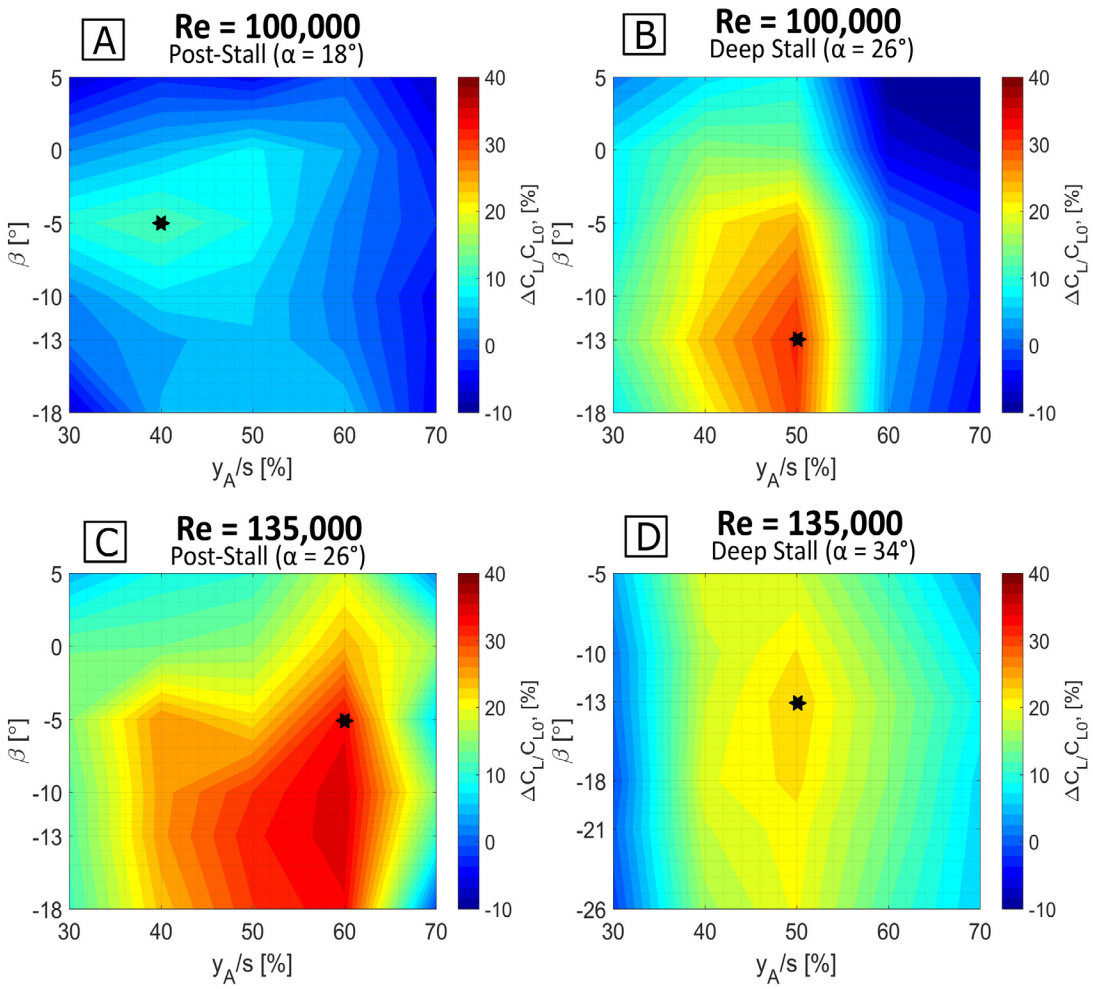

Figure 8. Contours of percent difference in lift coefficients generated by the baseline wing and the wing-LEAD assembly over y_A/s and β (A) and (B) at Re = 100 000 and (C) and (D) at Re = 135 000. Each plot shows the effect of varying the LEAD root location on lift. The contribution of γ is averaged. The results marked by a star represent the configurations tested for hot-wire anemometry.

the NACA22 airfoil, the LEAD as a lifting surface alone can add a maximum of 7% to the lift generated by the baseline wing. This value is driven by the difference in the wetted area of the LEAD compared to that of the wing. Based on the average obtained at Re = 100 000 post-stall, the lift improvement under this condition can be attributed to the LEAD as a lifting surface. Under the remaining conditions, the increase in lift are attributed to additional effects of the LEAD. The results in figure 7 confirm that the LEAD is a post-stall device in 3D (i.e. the device should only be deployed under post-stall conditions) These results agree with a previous experiment conducted by the authors on the wing-LEAD assembly in a 2D configuration as reported in [19, 20].

4.2. Effect of LEAD deployment parameters on lift

Based on the main effect results, only the forces generated at post-stall and deep stall AoAs are analyzed from this point forward. Figure 8 shows contours of $\%C_L$ ($\Delta C_L/C_{L0}$) across the LEAD relative angle of attack β and root location y_a/s at both Reynolds numbers. The effect of the alula tip deflection angle, γ has been averaged for these contour plots. Figures 8(A) and (B) show that at Re = 100 000, the lift difference generated by the wing-LEAD assembly increases as the LEAD root is moved outboard. The greatest increase in lift, 32%, occurs when the LEAD root is placed at 50% of semi-span under deep stall conditions ($\alpha = 26°$). Once the LEAD root location is moved outboard of this location, the lift enhancement declines but remains favorable compared to the baseline wing. At the most outboard location (70% semi-span away from the wing root), the LEAD tip protruded outboard of the wing tip, and most configurations generates lower lift coefficients than the baseline. The performance for the same configurations at Re = 135 000 is shown in figures 8(C) and (D). The results follow similar trends to that of Re = 100 000, except the location yielding the best performance is $y_A/s = 60\%$ under post-stall conditions. The greatest increase in lift, 29%, occurs when the wing is at post-stall. Similarly to Re = 100 000 results, lift enhancements declines as the LEAD is moved outboard of the location of highest improvement and lift penalties are observed at the outboard most location due to the tip of the LEAD protruding past the main wing tip. On average, the LEAD location that yields the highest lift is in the

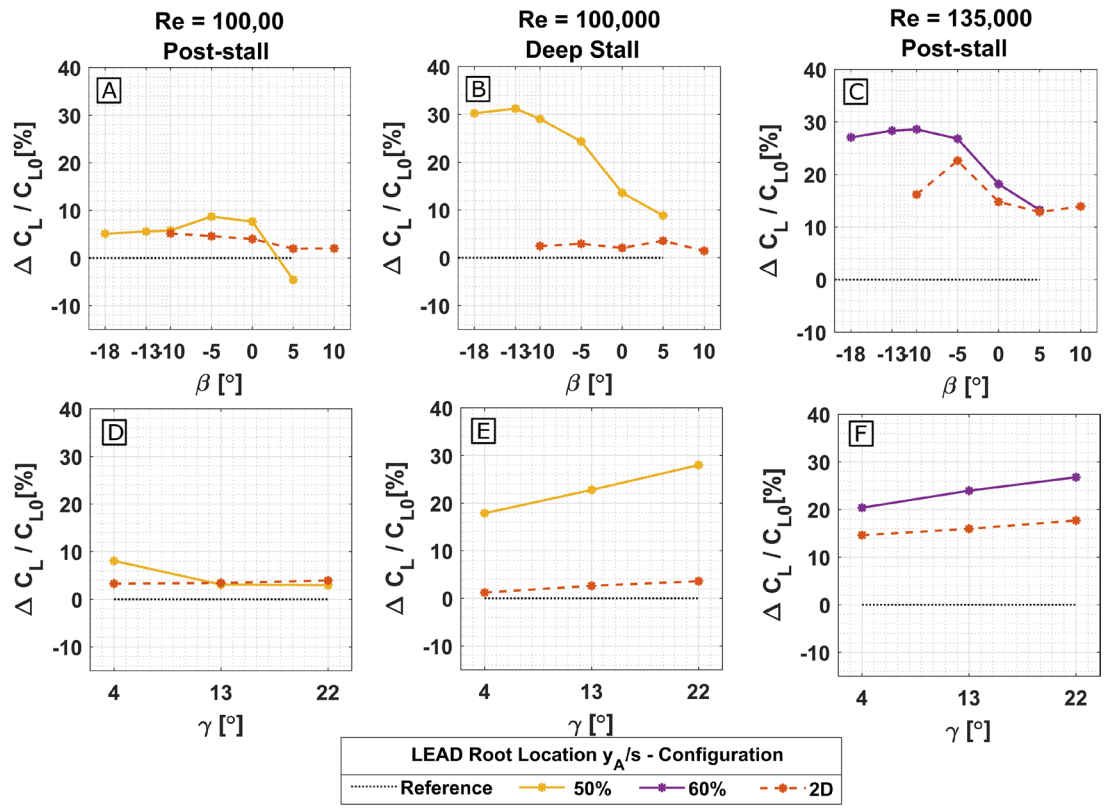

Figure 9. Comparison between lift percent differences generated by a LEAD on a wing (3D) and a LEAD on an airfoil (2D). Each curve represents the results at each root location. (A)–(C) Main effects of β with averaged γ. (D)–(F) Main effects of γ with averaged β. Adapted from [22].

middle of the semi-span (50%). This location is more outboard of the wing root when compared to the average alula location on type D avian wings. This difference may be due to the planform of the base wing, which has a uniform cross section and a rectangular profile. Nevertheless, the results in figure 8 indicates that lift is sensitive to the LEAD location.

Based on the LEAD lift effect sensitivity to location, a hypothesis was formulated that there are interactions between the LEAD tip vortices and the main wing tip vortices. This hypothesis was tested by comparing the lift obtained at the location (y_A/s) yielding the highest improvements against the lift generated by a 2D airfoil with a LEAD as tested by Mandadzhiev *et al* [19]. The 2D experiment took place in the same wind tunnel. The test setup was similar to the 3D experiments except the wing was confined with a wall on both sides to suppress 3D effects (shed tip vortices). Moreover, during the 2D test, the alula was mounted at the wing mid-span. Results in figure 9 indicate that the LEAD enhances lift production for both the 2D and 3D wing sections. However, the maximum lift improvement is always higher for the 3D wing. At Re = 100 000, the LEAD on a 2D wing yields C_l improvements ranging from 1% to 5% under both post-stall and deep stall conditions. The LEAD placed on a 3D wing improves the lift coefficient within ranges similar to the 2D configuration at post-stall. However, the LEAD enhances C_L significantly more under deep stall conditions, with lift enhancements ranging from 9% to 32%. At Re = 135 000, the 2D configuration yields an increase in lift, ranging from 11% to 22% at post-stall. The 3D wing configuration generates an increase of 11% to 29%. Overall, these results show higher lift enhancement when the LEAD is placed on a 3D wing as opposed to a 2D wing, confirming that the LEAD is a three-dimensional device. The results in figure 9 indicate that the interaction between the LEAD vortices and wing tip vortices contributes to the lift enhancement produced by the LEAD.

Figures 8 and 9 can be used to determine the sensitivity to the LEAD lift effect on the deployment parameters, namely, the LEAD relative angle of attack, β and tip deflection angle, γ. First, for the tip deflection angle, γ, higher values consistently yield greater lift enhancement. Second, even though most of the β values evaluated produce a positive percent change in C_L, the general trend of the contour plots in figures 8 and 9 is that lower (negative) β yield the best performance. At lower β values, the LEAD is at a low angle of attack relative to the freestream, thus it is less prone to separation itself. Therefore, the LEAD is more effective in producing lift and enhancing the flow around the wing. At Re = 100 000, the largest lift enhancement due to the LEAD is 32%, which occurs when the wing is at deep stall AoA (26°) and at Re = 135 000, the highest percent C_L obtained is 37%, which occurs when the wing is at post-stall AoA (26°). Both of these results

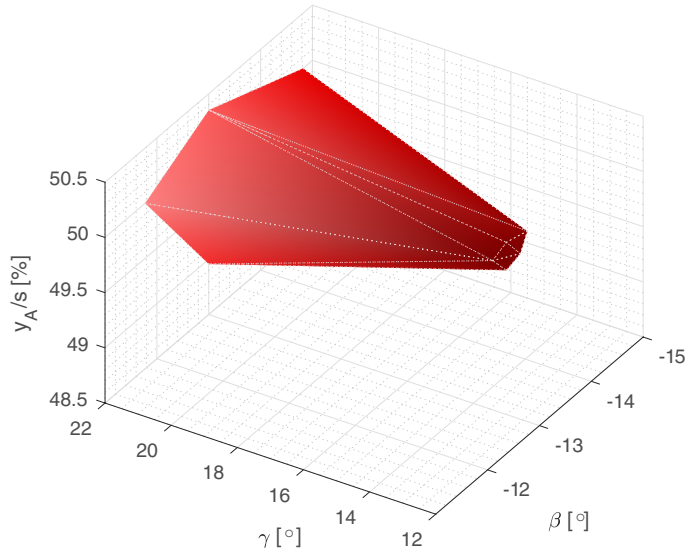

Figure 10. Isosurface at Re = 100 000 and under deep stall conditions ($\alpha = 26°$), showing a conical surface enclosing percent improvement in lift greater than 32%.

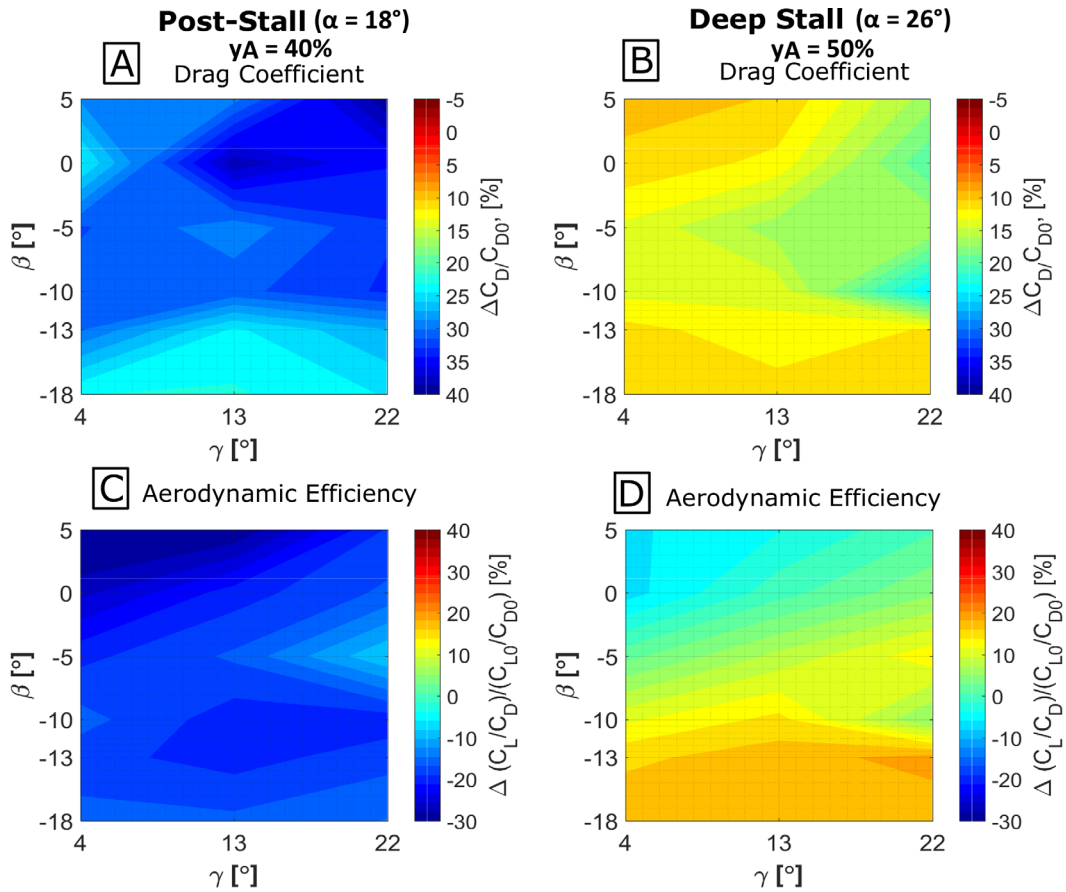

Figure 11. Contours of percent difference drag coefficients (A) and (B) and aerodynamic efficiency (C) and (D) generated by the baseline wing and the wing-LEAD assembly over β and γ at Re = 100 000. Despite generating a drag penalty, the LEAD maintains aerodynamic efficiency.

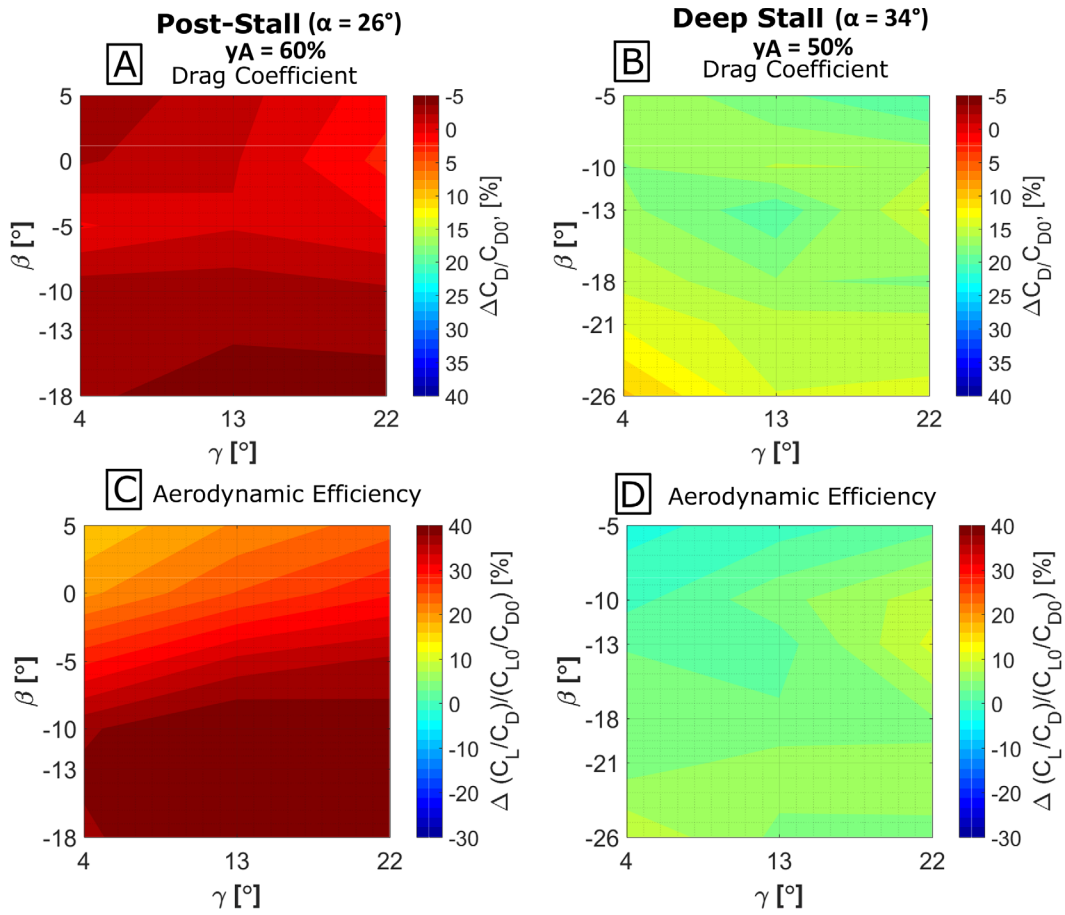

Figure 12. Contours of percent difference drag coefficients (A) and (B) and aerodynamic efficiency (C) and (D) generated by the baseline wing and the wing-LEAD assembly over β and γ at Re = 135 000. The LEAD decreases drag at post-stall AoA and increases aerodynamic efficiency at deep stall AoA.

occur at a negative β and a high γ irrespective of Reynolds number and main wing AoA.

However, the sensitivity on lift performance to the LEAD deployment parameters and LEAD location are not equal. For example, from figure 9, $\Delta C_L/C_{L0}$ is more sensitive to β than it is to γ. To illustrate this, the combination of the geometric parameters β, γ, and y_A/s that generate the lift improvements above 32% for Re = 100 000 and under deep stall conditions are shown in figure 10. The surface in this plot represents a threshold or a boundary in $\%C_L$ value. All configurations enclosed within the cone yield a lift increase greater than 32% and any configurations outside the cone do not satisfy the lift improvement criteria. Results show the ideal geometric parameters for the LEAD are: $-13.5° < \beta < -11.5°$, $15° < \gamma < 25°$, and $48.5\% < y_A/s < 50\%$. These results indicate that the LEAD root location and relative AoA needed to achieve a 32% lift improvement or greater fall within a narrow range. However, the range for the tip deflection angle is broader at approximately 10°. Additionally, the higher the γ value, the more the configurations that produce a C_L improvement of greater than 32%. Therefore, the lift generated by the wing-LEAD assembly is more sensitive to β and y_A/s than it is to γ.

4.3. Effects of the LEAD on drag and aerodynamic efficiency

Figures 11(A) and (B) shows contour representations of the percent difference in drag coefficient generated by the baseline and the wing-LEAD assembly ($\Delta C_D/C_{D0}$) over the deployment parameters β and γ at Re = 100 000. Figures 11(C) and (D) shows the same type of plots for aerodynamics efficiency or lift-to-drag ratio ($\Delta(C_L/C_D)/(C_{L0}/C_{D0})$). Drag and efficiency results are presented at post-stall and deep stall AoAs for the LEAD locations that produced the greatest lift enhancement. At post-stall AoA ($\alpha = 18°$), the LEAD generates a drag penalty, ranging from 23% to 39% for all configurations. The efficiency loss under this condition ranges from 8% to 32%. However, at the configuration that generated the highest lift coefficient ($\beta = -5°$ and $\gamma = 22°$), the aerodynamic efficiency is maintained with only an 8% loss. At deep stall AoA ($\alpha = 26°$), the LEAD generates a smaller drag penalty, ranging from 10% to 24%, and increased aerodynamic efficiency, ranging from a 7% loss to a 19% gain. When the highest lift improvement is obtained ($\beta = -13°$ and $\gamma = 22°$), the drag penalty is at 11% and the efficiency is improved at 19%. In this case, low β and all γ values produce a large region of low drag and high efficiency.

Figure 12 shows the same plots as above for the Re = 135 000 cases. At post-stall AoA ($\alpha = 26°$), the maximum drag penalty observed due to the LEAD is minimal at 2%. The drag coefficient is reduced by 5% in some configurations. Additionally, the aerodynamic efficiency also increases to a range of 16% to 40%. At the configuration that generated the highest lift coefficient ($\beta = -5°$ and $\gamma = 22°$), the drag penalty was as low as 0.5% and the aerodynamic efficiency as high as 36%. At deep stall AoA ($\alpha = 34°$), the LEAD also generates a small drag penalty, from 10% to 22%, but increases the aerodynamic efficiency, from a 2% loss to a 10% gain, for all configurations tested. When the highest lift improvement is obtained ($\beta = -13°$ and $\gamma = 22°$), the drag penalty is moderate at 14% and the efficiency is improved at 10%.

In general, despite the drag penalty generated when the LEAD is added to the system, aerodynamic efficiency is maintained and even improved in some cases. Additionally, a large combination of parameter generate low drag and high efficiency, reinforcing that the LEAD is suitable for mission-adaptability.

4.4. Effects of the LEAD on the wake

Hot-wire measurements were collected for the configurations underlined in table 2 and highlighted in figure 8. These measurements are used to provide insight on the integrated force measurements and to show the effect of the LEAD on the wake profile. Figure 13 shows velocity deficit profiles measured at various hot-wire probe locations across the span of the wing as illustrated in figure 5.

At Re = 100 000, under post-stall conditions (figure 13(A)), the velocity profile closest to the wing root (y = 0.25s) shows that the flow behind the wing decelerated to 30% of the freestream velocity ($0.3U_\infty$) for both the baseline and the wing-LEAD assembly. This deficit occurs from the upper wing surface (z = 0) to a height of z = 0.6c for both configurations. For the baseline case, the height of the velocity deficit gradually decreases as the probe is moved outboard, toward the wing tip. At the wing tip, the flow velocity is fully recovered to the freestream velocity (U_∞) along the entire profile. Adding the LEAD to the wing has no effects on the boundary layer at the probe locations inboard of the LEAD root. However, the deficit is reduced from a height of z = 0.5c (for baseline) to z = 0.2c (for wing-LEAD assembly) at y = 0.55s, which is the mid-LEAD location. Additionally, There is no difference observed in the velocity deficit profiles at the probe locations outboard of the LEAD tip.

At Re = 100 000 under deep-stall conditions (figure 13(B)), the velocity deficit profiles follow similar trends to the results under post-stall conditions. The only exception is observed at the LEAD root, where the velocity deficit increases from z = 0.4c (for baseline) to z = 0.8c (for wing-LEAD assembly). The increased deficit is caused by the LEAD connector disrupting the airflow when the wing is set to a larger AoA. However, this disruption does not affect the performance of the LEAD at any other locations. The flow is accelerated from 0.2 U_∞ (for baseline) to 0.5 U_∞ (for wing-LEAD assembly) at the mid-LEAD location and there are no noticeable differences between the baseline and the wing-LEAD assembly at the probe locations outboard of the LEAD tip.

At Re = 135 000 under post-stall conditions (figure 13(C)), the profile nearest to the wing root (y = 0.3s) shows that the flow decelerated to $0.15U_\infty$ behind both the baseline and the wing-LEAD assembly. This deficit occurs from the upper surface (z = 0) to a height of z = 0.65c for both configurations. Once again, the velocity deficit is the largest near the wing root and decreases toward the tip. Adding the LEAD to the wing has no effects on the boundary layer at the probe locations inboard of the LEAD root. At the LEAD root, the deficit increases from a height of z = 0.15c (for baseline) to z = 0.6c (for wing-LEAD assembly) due to the LEAD connector. However, at the mid-LEAD location, y = 0.75s, the deficit is reduced from a height of z = 0.05c (for baseline) to z = 0c (for wing-LEAD assembly) and the flow is accelerated from 0.4 U_∞ (for baseline) to 0.6 U_∞ (for wing-LEAD assembly) at the mid-LEAD location and there are no noticeable differences at the probe locations outboard of the LEAD tip. Lastly, there are no noticeable differences between the baseline and the wing-LEAD assembly at the probe locations outboard of the LEAD tip.

Under deep stall conditions at Re = 135 000 (figure 13(D)), the deficit profile nearest to the wing root (y = 0.35s) shows that the flow has decelerated to $0.15U_\infty$ in the wake of the baseline and wing-LEAD assembly. This deficit occurs from z = 0 (upper surface) to a height greater than z = 0.8c for both configurations. Once again, the size of the velocity deficit profile decreases as the hot-wire is moved outboard along the span. However, for the baseline, the wake velocity profile never recovers to freestream (U_∞) at the wing tip. In fact, the velocity deficit profile is as large as z = 0.6c at this location. Adding the LEAD to the wing has a similar effect to the previous cases inboard of the LEAD and at its root. At y = 0.65s (mid-LEAD location), the height of the deficit profile remains unchanged, but the flow is accelerated from 0.3 U_∞ to 0.5 U_∞. At the LEAD tip, the deficit profile height is reduced from 0.8c in the baseline to 0.15c in the wing-LEAD configuration. Moreover, the flow velocity is fully recovered to freestream (U_∞) for the wing-LEAD assembly at the wing tip. The reduction in velocity deficit due to the LEAD become more pronounced as the probe location is moved outboard of the LEAD.

In figures 13(A)–(C), the largest flow deficit in the wake of the baseline wing is observed at the root and decreases in height outboard until no deficit is observed at or near the wing tip. This trend indicates partial stall over the wing. After adding the LEAD, no wake effects are observed at probe locations inboard of the LEAD root. Outboard of the LEAD tip, even

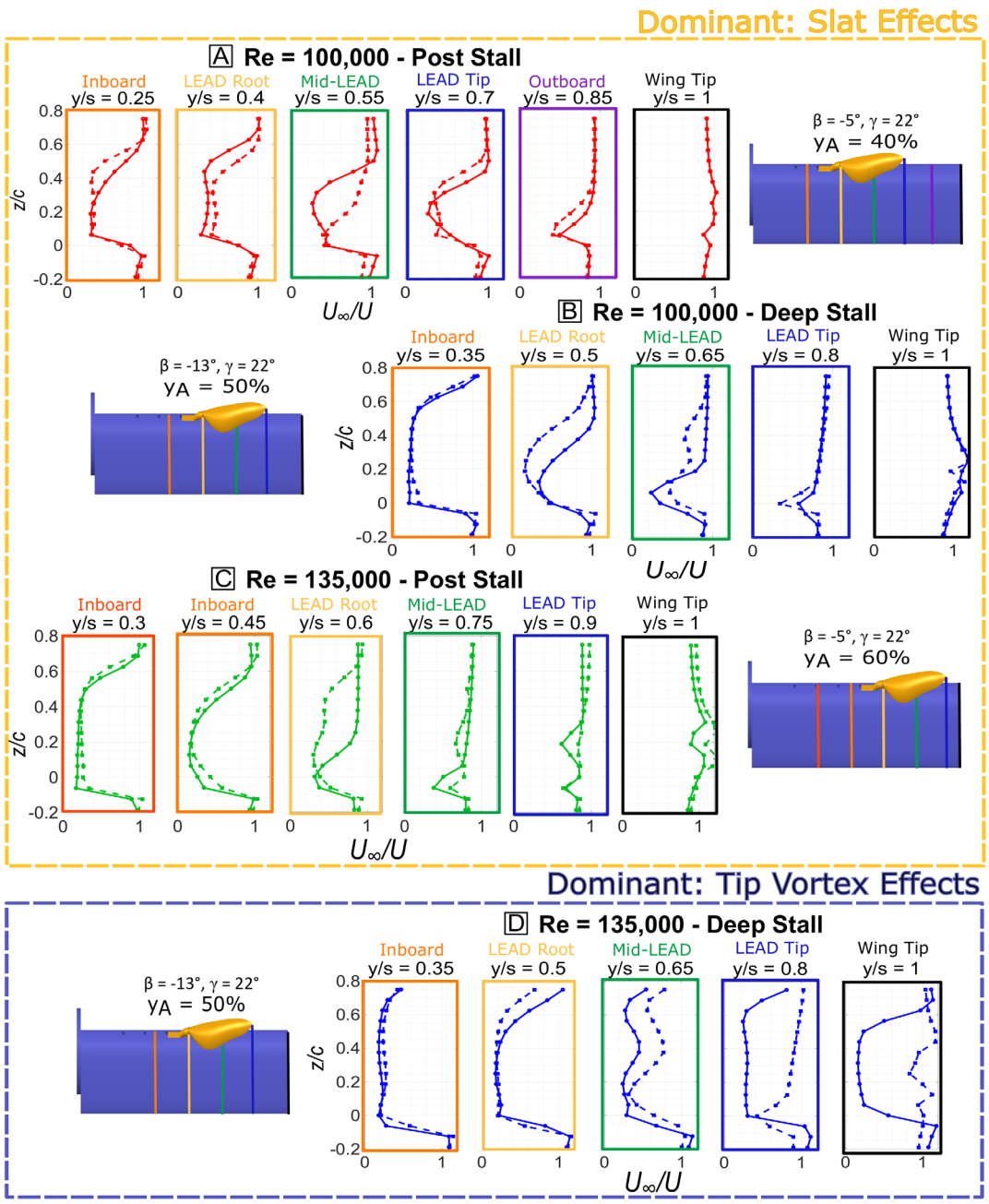

Figure 13. Velocity deficit profiles in the wake of the baseline and the wing-LEAD assembly. The baseline profiles are represented by solid lines, and the wing-LEAD assembly profiles are represented by dashed lines. The LEAD accelerates the flow in the wake and reduces the wake deficit. Two main effects are presented: slat effect and tip vortex effect.

though the device sheds a tip vortex, its effects of the wake are negligible because the flow over the wing attached in this region. However, the airflow accelerates, and separation is alleviated in the region behind the LEAD. This behavior is comparable to traditional leading-edge slats. In this configurations, the LEAD generated a drag penalty while maintaining aerodynamic efficiency. Moreover, when the LEAD decreased the velocity deficit the most (figure 13(C)), the largest decrease in drag as well as an increase in the aerodynamic efficiency were also observed. Results from figures 13(A)–(C) indicate that when the main wing is under partial stall flow conditions, like a slat, the LEAD accelerated the flow over the upper surface of the wing, causing an increase in lift.

In figure 13(D), the flow in the wake of the baseline wing is separated from root to tip, indicating that the wing is fully stalled. In this case, the LEAD reduces the velocity deficit not only in the region it occupies, but also at locations outboard of its tip. While the slat effect is still present, the LEAD tip vortex effects become apparent. These effects are due to a streamwise vortex shed at the LEAD tip that adds momentum to the flow on the wing upper surface. Thus, for fully stalled

wings, the LEAD acts as a boundary layer fence that prevents flow separation from propagating outboard of the LEAD. These results are consistent with the DPIV observations made by Lee *et al* [7] and confirm that there are interactions between the tip vortex shed by the LEAD and the tip vortex shed by the main wing.

5. Conclusion

This paper presents a complete set of integrated and distributed flow measurements for a leading-edge device inspired by the alula feathers of birds on a three dimensional wing. The effects of the device on lift and drag production and the wake velocity profile are presented. Integrated force measurements show the following:

- In general, the LEAD improves lift under post and deep stall conditions but decreases lift at pre-stall AoAs. This indicates that the LEAD is a post-stall device
- The percent change in lift generated by the wing-LEAD assembly, as compared to baseline, is sensitive to the spanwise LEAD location. The largest improvements are produced when the LEAD is placed near the middle of the semi-span of the wing.
- The LEAD produces higher percent lift improvements when implemented on a moderate aspect-ratio wing (3D) compared to an airfoil (2D) test section, indicating that there is an interaction between the LEAD vortices and the wing tip vortices.
- The lift improvement produced by the LEAD is sensitive to its morphological deployment parameters. Measurements indicate that the LEAD performance is more sensitive to relative AoA (β) and spanwise location (y_A/s) than to tip deflection angle (γ)
- Despite some drag penalty generated, the wing maintains aerodynamic efficiency when the LEAD is added.

Hot-wire anemometer measurements show that, for partially stalled wings, the LEAD reduces the wake velocity deficit and delays flow separation similar to traditional leading-edge slats. On fully stalled wings, the LEAD does not only act as a leading-edge slat, but also creates the boundary layer fence that prevents the propagation of stall outboard of the LEAD root. Thus, the two major effects of the LEAD on a moderate aspect-ratio wing can be classified as lift enhancement and stall mitigation.

In nature, the alula is an adaptive and flexible high-lift device that is only deployed at steep AoAs and during flight tasks that require high maneuverability. While this paper successfully adapted the alula function to an engineered wing using a static device, future work includes designing a deployment mechanism for the LEAD that can respond to dynamic flow conditions. The development of a dynamic LEAD creates an opportunity for improved maneuverability and mission adaptability for UAVs that operate at low Reynolds number. Such device would enable short-distance take-off and landing, perching maneuvers, and resistance to gusts and changing flow conditions.

Acknowledgments

The authors would like to acknowledge and thank the Mechanical Science and Engineering Department at the University of Illinois at Urbana-Champaign for continued support and resources. The authors would also like to thank the Renewable Energy & Turbulent Environment Group for their input on the hot-wire anemometer experiments.

ORCID iDs

Mihary R Ito https://orcid.org/0000-0002-9283-4891
Aimy A Wissa https://orcid.org/0000-0002-8468-511X

References

[1] Weibel R E and Hansman R E 2004 Safety considerations for operation of different classes of UAVs in the NAS *AIAA 3rd "Unmanned Unlimited" Technical Conference, Workshop and Exhibit (Chicago, IL, USA, 20–23 September 2003)* (https://doi.org/10.2514/6.2004-6421)
[2] Mohamed A, Massey K, Watkins S and Clothier R 2014 The attitude control of fixed-wing MAVS in turbulent environments *Prog. Aerosp. Sci.* **6** 37–48
[3] Anderson J D 2009 *Fundamentals of Aerodynamics* (*McGraw-Hill Series in Aeronautical and Aerospace Engineering*) 5th edn (Boston, MA: McGraw-Hill)
[4] Lissaman P B S 1983 Low-Reynolds-number airfoils *Annu. Rev. Fluid Mech.* **15** 223–39
[5] Withers P C 1981 An aerodynamic analysis of bird wings as fixed aerofoils *J. Exp. Biol.* **90** 143–62
[6] Tobalske B 2000 Biomechanics and physiology of gait selection in flying birds *Physiol. Biochem. Zool.* **73** 736–50
[7] Lee S-I, Kim J, Park H, Jabłoński P G and Choi H 2015 The function of the alula in avian flight *Sci. Rep.* **5** 9914
[8] Meseguer J, Franchini S, Pérez-Grande I and Sanz J L 2005 On the aerodynamics of leading-edge high-lift devices of avian wings *Proc. Inst. Mech. Eng. G* **219** 63–8
[9] Austin B and Anderson A M 2008 The alula and its aerodynamic effect on avian flight *ASME Int. Mechanical Engineering Congress and Exposition* (https://doi.org/10.1115/IMECE2007-41693)

[10] Videler J J 2005 *Avian Flight* (Oxford: Oxford University Press)
[11] Savile D B O 1957 Adaptive evolution in the avian wing *Evolution* **11** 212–24
[12] Liu T, Kuykendoll K, Rhew R and Jones S 2006 Avian wing geometry and kinematics *AIAA J.* **44** 954
[13] Álvarez J C, Meseguer J, Meseguer E and Pérez A 2001 On the role of the alula in the steady flight of birds *Ardeola* **48** 161–73
[14] Nachtigall W and Kempf B 1971 Vergleichende untersuchungen zur flugbiologischen funktion des daumenfittichs (alula spuria) bei vgeln *Z. Vergleichende Physiol.* **71** 326–41
[15] Weyl A R 1945 High-lift devices and tailless aeroplanes *Aircr. Eng. Aerosp. Tech.* **17** 325–30
[16] Smith A M O 1975 High-lift aerodynamics *J. Aircr.* **12** 30–50
[17] Abbott I H and Von Doenhoff A E 1959 *Theory of Wing Sections: Including a Summary of Airfoil Data* (New York, NY: Dover Publications)
[18] Rao D and Kariya T 1988 Boundary-layer submerged vortex generators for separation control—an exploratory study *1st National Fluid Dynamics Conf. (Reston, Virigina 1988)* (American Institute of Aeronautics and Astronautics) (https://doi.org/10.2514/6.1988-3546)
[19] Mandadzhiev B A, Lynch M K, Chamorro L P and Wissa A A 2017 An experimental study of an airfoil with a bio-inspired leading edge device at high angles of attack *Smart Mater. Struct.* **26** 094008
[20] Mandadzhiev B A, Lynch M K, Chamorro L P and Wissa A A 2016 Alula-inspired leading edge device for low Reynolds number flight *Proc. of the ASME 2016 Conf. on Smart Materials, Adaptive Structures and Intelligent Systems. Volume 2: Modeling, Simulation and Control; Bio-Inspired Smart Materials and Systems; Energy Harvesting.* (Stowe, Vermont, USA, September 28–30 2016) V002T06A016
[21] Mandadzhiev B A Design and aerodynamic analysis of an airfoil with a bioinspired leading- edge device for stall mitigation at low Reynolds number operations *PhD Thesis* Department of Aerospace Engineering, University of Illinois at Urbana-Champaign
[22] Ito M R, Duan C, Chamorro L P and Wissa A A 2018 A leading-edge alula-inspired device (LEAD) for stall mitigation and lift enhancement for low Reynolds number finite wings *Proc. of the ASME 2018 Conf. on Smart Materials, Adaptive Structures and Intelligent Systems. Volume 2: Mechanics and Behavior of Active Materials; Structural Health Monitoring; Bioinspired Smart Materials and Systems; Energy Harvesting; Emerging Technologies. (San Antonio, TX, USA, September 10–12 2018)* (ASME) V002T06A011
[23] Sander A 2018 The role of the alula in avian flight and its application to small aircraft: a numerical study *MS Thesis* University of Groningen, Groningen, Netherlands (https://doi.org/10.13140/RG.2.2.34539.18724)
[24] Carruthers A C, Walker S M, Thomas A L R and Taylor G K 2010 Aerodynamics of aerofoil sections measured on a free-flying bird *Proc. of the Inst. of Mechanical Engineers, Part G: Journal of Aerospace Engineering* **224** 855–64